

# Results From E-810 Concerning Strange Particles and Strangelet Search\*

R.S. Longacre<sup>a</sup>, S. Ahmad<sup>d</sup>, B.E. Bonner<sup>d</sup>, J.A. Buchanan<sup>d</sup>, C.S. Chan<sup>b</sup>, C.N. Chiou<sup>d</sup>, J.M. Clement<sup>d</sup>, E. Efstathiadis<sup>b</sup>, S.E. Eiseman<sup>a</sup>, A. Etkin<sup>a</sup>, K.J. Foley<sup>a</sup>, R.W. Hackenburg<sup>a</sup>, T.J. Hallman<sup>c</sup>, M.A. Kramer<sup>b</sup>, S.J. Lindenbaum<sup>a,b</sup>, W.A. Love<sup>a</sup>, L. Madansky<sup>c</sup>, T.W. Morris<sup>a</sup>, G.S. Mutchler<sup>d</sup>, E.D. Platner<sup>a</sup>, A.C. Saulys<sup>a</sup>, K. Zhao<sup>b</sup>, and Y. Zhu<sup>b</sup>

<sup>a</sup>Brookhaven National Laboratory, Upton, NY 11973 USA

<sup>b</sup>City College of New York, New York, NY 10031 USA

<sup>c</sup>Johns Hopkins University, Baltimore, MD 21218 USA

<sup>d</sup>Rice University, Houston, TX 77251 USA

We present the results of  $\Lambda$  and  $K^0$  production from a  $Si$  target with a  $14.6 \times A$  GeV/c  $Si$  beam. The measured rapidity distribution and transverse mass exponential slopes are presented and compared with models. We also present a measurement of  $\Xi^-$  production from a  $Pb$  target with the same beam. The rapidity distribution is measured along with a model comparison. Finally we have searched for strangelets which decay in our TPC volume. From a Monte Carlo study with a plasma production model, we have established a upper limit on a given strangelet production cross section.

## 1. INTRODUCTION

There is considerable interest in studying strange particle production in heavy ion interactions, since enhancement of strangeness production over that expected from a superposition of nucleon-nucleon interactions has been reported by several experiments.[1-4] Enhanced strange particle production in heavy ion interactions has been suggested as one of the signals of quark-gluon-plasma (QGP) formation.[5] Also the formation of strange matter droplets (strangelets) is another signal that the QGP has been formed and strange quarks have been distilled in the presence of large chemical potential.[6]

## 2. EXPERIMENTAL METHOD

The experimental method was described in previous publications.[4,7] Briefly, experiment E-810 measured charged tracks in three TPC (Time Projection Chamber) modules in a magnetic field. The detector covered the forward hemisphere in the center-of-mass of the nucleon-nucleon system. The trigger, as described in Ref. 4, selected centrally enriched events for data recording. For the final data sample we selected the most central events using a cut on the highest multiplicity of the negatively charged tracks with in

---

\* This research was supported by the U.S. Department of Energy under Contract Nos. DE-AC02-76CH00016, DE-FG02-91ER40645, DE-FG02-88ER40413, DE-FG05-87ER40309, and the City University of New York PSC-BHE Research Award Program.

our good acceptance. The selection corresponded to a cross section of 100 mb for the silicon target and 300 mb for lead. These cuts correspond to approximately 10% of the geometric cross section. The effective masses for  $K_s^0$ 's and  $\Lambda$ 's were calculated by kinematic hypothesis by assigning a proton or a pion mass to the charged tracks which form a vertex.

Figure 1a shows the results of the effective mass calculation for the  $\pi^+\pi^-$  hypothesis and Fig. 1b shows the results of the  $p\pi^-$  hypothesis for our final selected data sample from the  $Pb$  target. Decay vertices with effective masses in the range of 0.475–0.525  $\text{GeV}/c^2$  were selected as  $K_s^0$ 's and those in the range of 1.106–1.126  $\text{GeV}/c^2$  were selected as  $\Lambda$ 's.

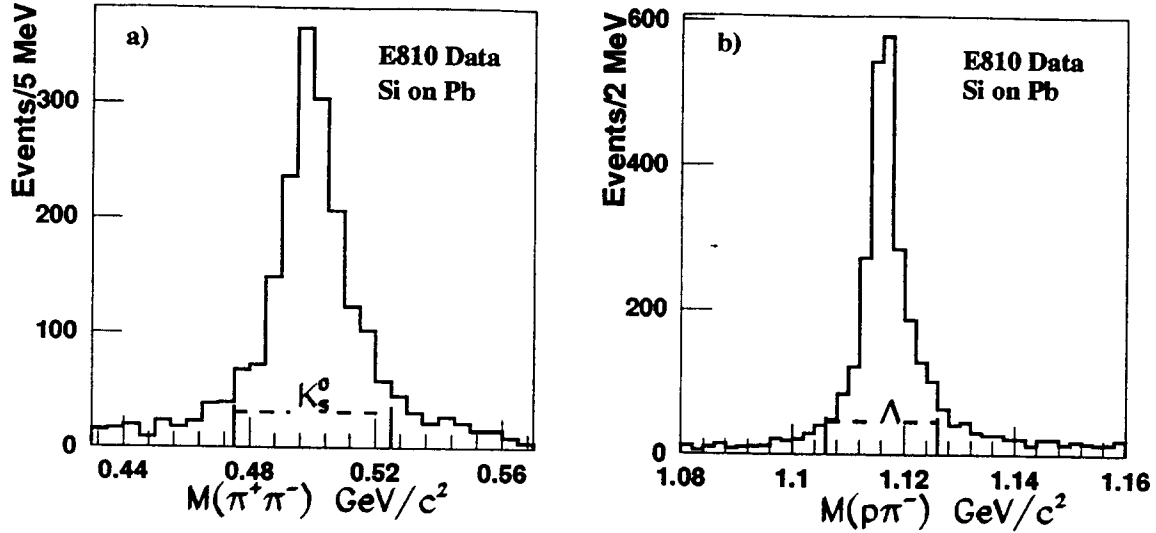


Fig. 1: (a) Effective mass plot of  $\pi^+\pi^-$  hypothesis for the decay vertices from  $Pb$  target with vertices removed if they satisfy the  $\Lambda$  effective mass cuts. (b) Effective mass plot of the  $p\pi^-$  hypothesis for decay vertices from  $Pb$  target.

### 3. $K_s^0$ AND $\Lambda$ RESULTS

In this report we present the results of 817  $K_s^0$ 's produced from a  $14.5 \times A$   $\text{GeV}/c$   $Si$  on a  $Si$  target with rapidity  $2.0 < y < 3.5$ , and 1122  $\Lambda$ 's in the rapidity range of  $1.4 < y < 3.2$ .

In order to extrapolate to unmeasured regions of the transverse momentum  $p_t$  we have fitted our acceptance corrected data to

$$\frac{1}{m_t} \frac{d^2 N}{dy dm_t} = A \exp(-B m_t) \quad (1)$$

where,  $m_t = \sqrt{p_t^2 + m_0^2}$ . We choose to extrapolate in order to present rapidity distributions, instead of using an integral only over our measured transverse momentum range of  $p_t < 1.0$   $\text{GeV}/c$ . We have performed a fit using the hypothesis,  $A$  as an arbitrary constant independent of rapidity and  $B$  takes the form of  $B = a + b \cosh(y - y_0)$  where  $a$  and  $b$  are independent of rapidity (fireball model).[8] In our fit to  $Si$   $Si$ , we obtain a global parameterization of the  $K_s^0$  and  $\Lambda$  data.

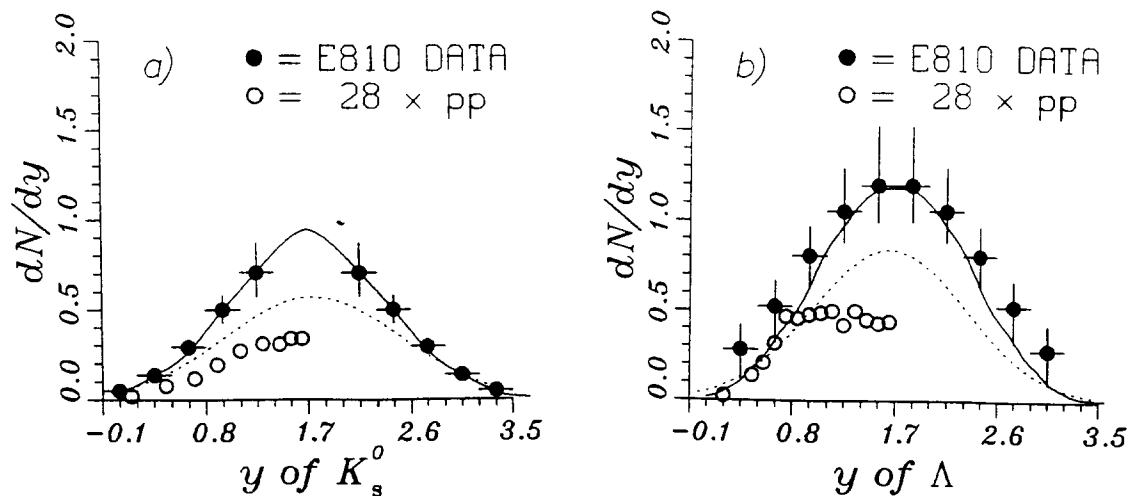


Fig. 2: (a) Rapidity distribution for  $K_s^0$ 's from the  $Si$  target. The solid points above a rapidity of 1.7 are our measurements. Errors shown are statistical only. The solid points below rapidity of 1.7 are our data reflected about 1.7. The open circles represent the measurements of Ref. 9 scaled by 28. The solid curve is the prediction of the RANDOM model. The dotted curve is the prediction of the HIJET with  $N^*$  model. (b) Rapidity distribution for  $\Lambda$ 's from the  $Si$  target.

In Fig. 2 we plot the rapidity distribution for  $K_s^0$ 's and  $\Lambda$ 's from the  $Si$  target. The curves shown in the figures are the predictions of two models. Also shown are the measured rapidity distributions[9] for  $p + p \rightarrow K_s^0 + X$  and  $\rightarrow \Lambda + X$  at 12 GeV/c scaled up by a factor of 28. The rapidity distributions were measured only for forward rapidities, but reflected about  $y = 1.7$  (corresponds to  $\sim y = 0$  in the  $N-N$  c.m.s.). The first thing to be noted is that our  $Si$  data cannot be described by the naive assumption that we can scale up the  $pp$  cross section by 28. AGSHIJET+ $N^*$ [10] seems to do a reasonable job of predicting the  $K_s^0$  rapidity but falls short for  $\Lambda$  rapidity. AGSHIJET+ $N^*$  uses geometry and cross sections to determine if collisions take place. In order to gain insight we have used a simpler model called RANDOM which uses the scattering routines of HIJET but scatters pairs of particles randomly with probabilities proportional to their total cross section. The number of collisions per event is an input parameter. We have chosen the number of collisions that gives a good agreement with the RQMD proton  $dn/dy$  of Ref. 11 for  $Si Si$  at AGS energies (320 col/event gives proton  $dn/dy = 10$  at  $y = 1.7$ ). The time between collisions is another variable which must be adjusted in the RANDOM model. We adjusted the time to be around 1/3 fermi so that the Boltzman temperature of the central rapidity protons would be around 200 MeV. In Fig. 3, we show the inverse slopes from our  $Si Si$   $K_s^0$  and  $\Lambda$  data as a functions of rapidity. The dashed curve is the cosh  $(y - y_0)$  global fit described above. The RANDOM model does a good job in describing both the  $K_s^0$ 's and  $\Lambda$ 's and can give us some insight into why AGSHIJET+ $N^*$  fails to describe the data.  $\Lambda$ 's are formed in HIJET from initial collisions and thus have limited  $P_t$  or later on by secondary interactions and have limited  $P_t$  because they have the greatest cross section to be formed by associated production near the  $K \Lambda$ [10] threshold. In Fig. 4a, we show the inverse slope for  $\Lambda$ 's coming from the RANDOM model after different

number of collisions. After 50 collisions the  $\Lambda$ 's are all fresh and their inverse slope is the same as HIJET produces. As collisions continue  $\Lambda$ 's are heated up by collisions with nucleons and become more thermal in nature. Finally Fig. 4b shows the  $\pi^-$  spectrum from E-810 Si Si central collision and compares them with the RANDOM model.

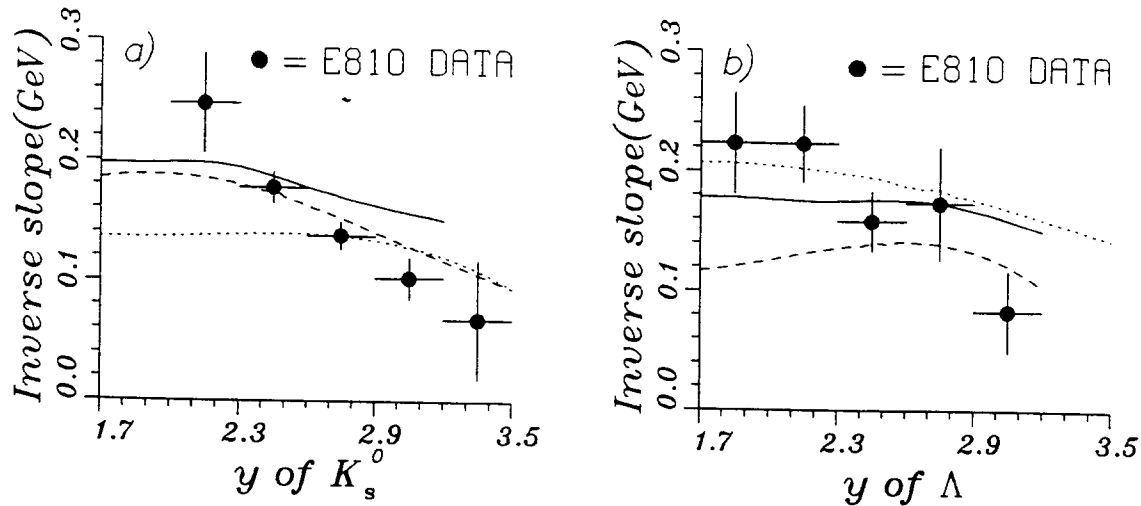


Fig. 3: (a). Inverse exponential slopes for  $K_s^0$ 's from the Si target. The solid points are our measurements, where the errors shown are statistical only. The dashed curve is the result of our global fit. The solid curve is the prediction of the RANDOM model. The dotted curve is the prediction of the HIJET with  $N^*$  model. (b) Inverse exponential slopes for  $\Lambda$ 's from the Si target.

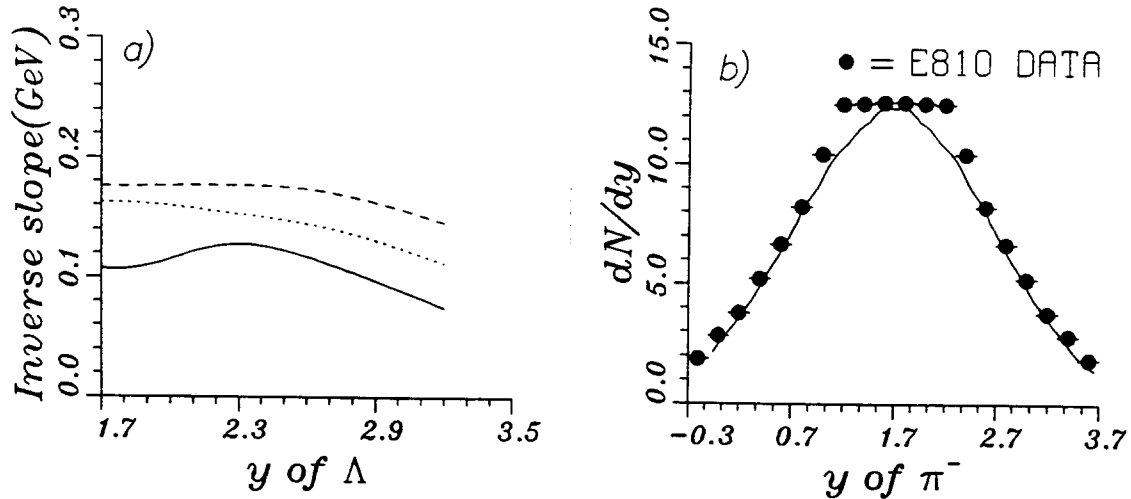


Fig. 4: (a) Inverse exponential slopes for  $\Lambda$ 's from the Si target coming from the RANDOM model. The solid curve is the slope after 50 collisions per event. The dotted curve is the slope from 150 collisions per event. The dashed curve is the slope from 250 collisions per event. (b) Rapidity distribution for  $\pi^-$  from the Si target. The solid points above a rapidity of 1.7 are our measurements. Errors shown are statistical only. The solid curve points below rapidity of 1.7 are our data reflected about 1.7. The solid curve is the prediction of the RANDOM model.

#### 4. $\Xi^-$ RESULTS

We have successfully found a  $\Xi^-$  signal in our *Si Pb* data. The procedure for finding the  $\Xi^-$ 's starts by considering only tracks that are well measured (sagitta  $> 0.375$  cm). From positives and negatives we find  $\Lambda$ 's which miss the primary target by 0.25 cm. We project the  $\Lambda$ 's path back up stream and search for negative tracks that come within 0.4 cm of the projection. We then swim the resulting negative particle back toward the primary vertex ( $\sim 44$  cm). If the decay position of the  $\Xi^-$  lies between  $50 < z < 60$  cm, we require that the  $\Xi^-$  passes within 0.6 cm of the primary vertex. If the  $\Xi^-$  decays after 60 cm, we require that it pass within 1.0 cm of the primary vertex. The effective mass distribution of the  $\Lambda \pi^-$  is given in Fig. 5a. We select  $\Xi^-$ 's that lie in the range  $1.306 < M(\Lambda \pi^-) < 1.336$   $\text{GeV}/c^2$ .

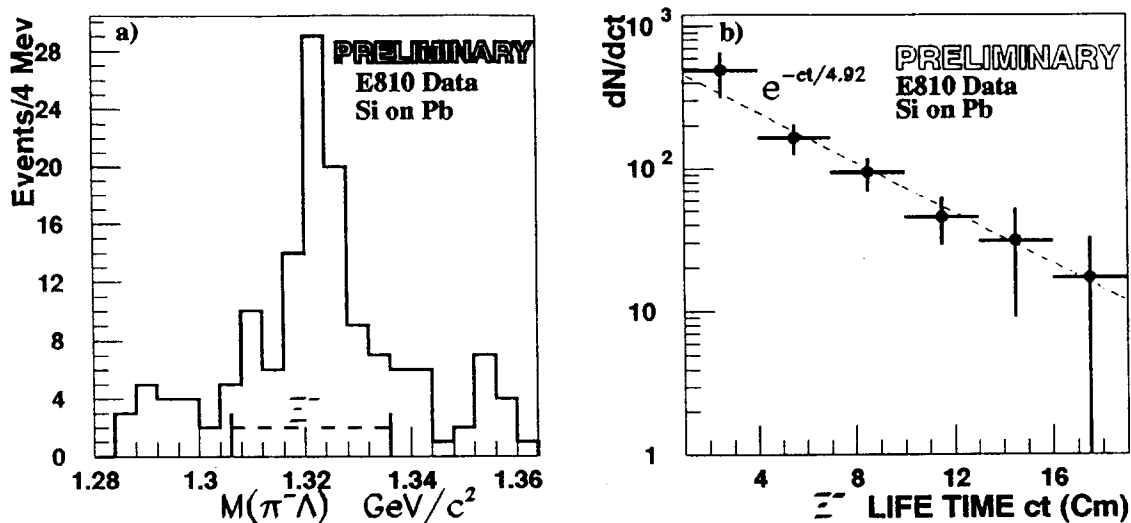


Fig. 5: (a) Effective mass plot of  $\Lambda \pi^-$  hypothesis for the intersection of a negative track with the projection of the  $\Lambda$  decay vertices from *Pb* target. (b) The  $\Xi^-$  decay distribution from central events in the *Pb* target. The dashed curve is the known measured value  $e^{-ct/4.92}$ .

In order to calculate acceptances, a complete Monte Carlo simulation of events was performed using GEANT. Events were generated using the HIJET model. The generated TPC's hits included all the known effects of the detector apertures, efficiencies, resolutions, and distortions. The  $\Xi^-$  lifetime is well known and the acceptance corrected decay distribution as a function of proper time can be calculated. Figure 5b shows this distribution and it is in good agreement with the measured value plotted in this figure. This gives us confidence in our acceptance calculations. The acceptance corrected rapidity spectrum for the  $\Xi^-$ 's is shown in Fig. 6a along with 4 times the rapidity spectrum as generated by HIJET. This production is equal to 0.2  $\Xi^-$ 's per central event. HIJET underestimates the production of strange particles with one strange quark by a factor of two.[7] If we conclude that there is a scale of two for each strange quark, HIJET's factor of four underestimation of  $\Xi^-$ 's seems predictable. On the other hand, HIJET does a poor job at representing the transverse mass distribution of the  $\Lambda$ 's. When we used the acceptance derived from HIJET  $\Lambda$ 's only, it appeared that HIJET agreed with the data[4]. If we would use the global form derived from the  $\Lambda$  data, the acceptance may fall by another factor of two

thus implying a factor 8 and a production of about one  $\Xi^-$  for every two central  $Si Pb$  event.

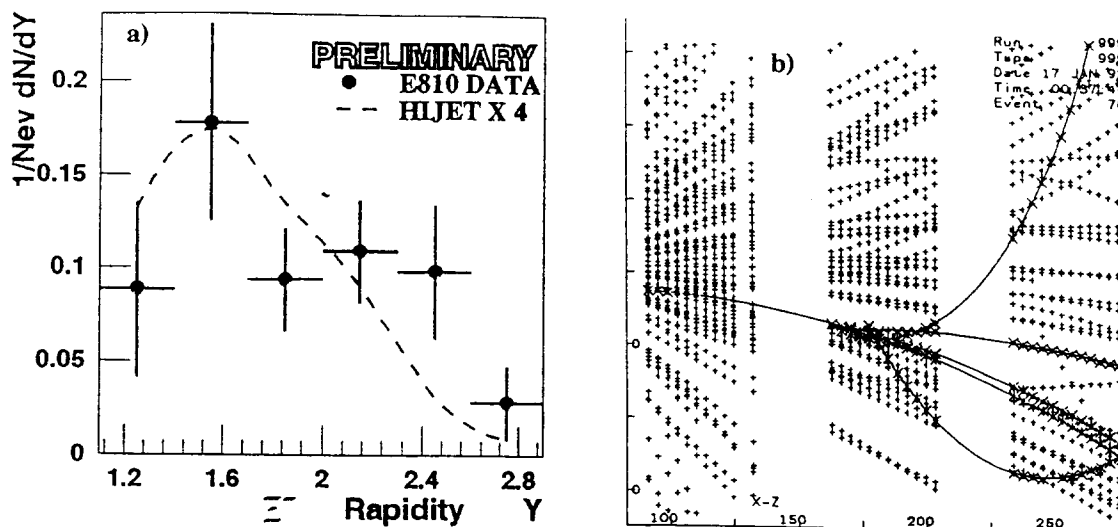


Fig. 6: (a) Rapidity distribution for  $\Xi^-$ 's from the  $Pb$  target. The dashed curve is four times the prediction of HIJET with  $N^*$  model. Errors shown are statistical only. (b) The  $X-Z$  view of a Monte Carlo event from  $Si Pb$  in our three TPC modules, where the tracks of the strangelet are shown and the others have been removed.

## 5. SEARCH FOR METASTABLE STRANGELETS

It has been proposed that quark matter with finite net strangeness might be metastable with respect to the strong interaction.[12] Such "strangelets", i.e., blobs of multistrange quark matter, if detected, would most probably be the only form of quark matter not subject to rapid decay.

Greiner, Koch, and Stöcker[6] demonstrate that, during the QGP phase transition into a HG (Hadron Gas) phase a large antistrangeness content will build up in the HG phase while a large strangeness excess will be left in the QGP phase. This excess during hadronization could form into strangelet blobs of quark matter. Most likely the strangelet blobs will decay by the weak decay with a lifetime of the order or greater than the  $\Lambda$  lifetime which is  $\sim 1/4$  nanosecond. The decay products will consist of hyperons plus other particles like pions and nucleons. The hyperons then travel away from this vertex and decay forming secondary vertices. In our data we explored two related topologies which consist of a primary  $V$  followed by a secondary  $V$  which points back to it. This topology consists of a neutral strangelet which decays by virtual  $\Lambda$  decay thus creating a  $\pi^-$ , a  $p$ , a  $\Lambda$ , and possible neutrals. The secondary  $\Lambda$  travels some distance and then decays into another  $V$  consisting of a  $\pi^-$  and a  $p$ . Another related topology consists of a single charged positive strangelet which decays by virtual  $\Lambda$  into a  $\pi^-$ , two  $p$ 's, a  $\Lambda$ , and possible neutrals.

In order to conduct a search for strangelets, we have made a complete Monte Carlo simulation of central  $Si Pb$  (HIJET) events with an embedded strangelet which has a strangeness of two, baryon number of three, and a charge of one. We have used a lifetime

of three nanoseconds which maximizes the number decaying in our TPC. GEANT was modified so that it would correctly decay the strangelet. These GEANT tracks were made into TPC hits and included all the known effects. A pattern recognition algorithm was developed to find the Monte Carlo generated strangelets (see Fig. 6b). Figure 7a shows the effective mass spectrum of Monte Carlo events for the double  $V$ 's. We observe a peak at effective mass equal to  $2.21 \text{ GeV}/c^2$ . We next show the effective mass adding the proton to the vertex (Fig. 7c). We obtain a peak at  $3.15 \text{ GeV}/c^2$ , which consistent with the strangelet mass put into the Monte Carlo. The acceptance for the above events is around 2% assuming the plasma bubble distillation of our model (central rapidity - low  $P_t$ ), the  $\Lambda p p \pi^-$  is 64% of the total (virtual  $\Lambda$  has same ratio as  $\Lambda$ ), and  $p p p \pi^- \pi^-$  is 41% of the total.

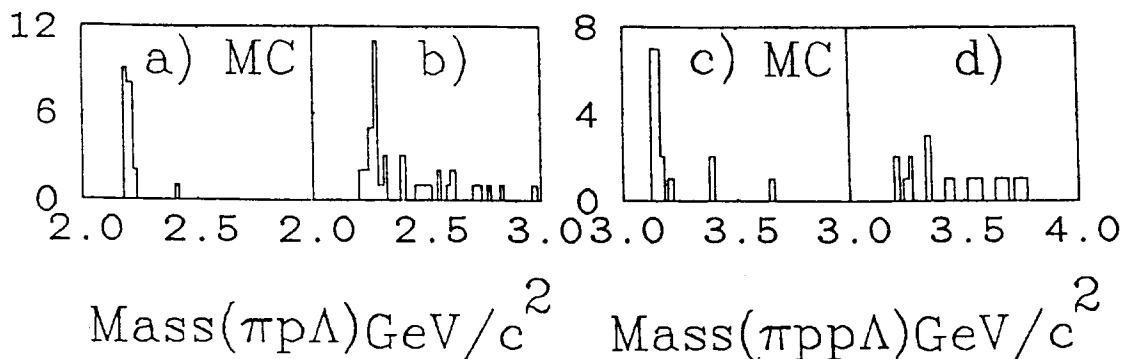


Fig. 7: (a) The effective mass of the double  $V$ 's from Monte Carlo generated  $Si Pb$  central events. (b) The effective mass of the double  $V$ 's from our  $Si Pb$  central events. (c) the effective mass of the double  $V$ 's with an added proton from Monte Carlo generated central  $Si Pb$  events. (d) the effective mass of the double  $V$ 's with an added proton from our central  $Si Pb$  events.

We have made a search over  $\sim 10,000$  central  $Si Pb$  events and our results for double  $V$ 's are shown in Fig. 7b. We have 41 entries and do not observe a peak below the  $\Lambda\Lambda$  threshold. We do however observe a peak at  $2.26$  with width of  $\sim 50 \text{ MeV}/c^2$ . If we make an effective mass spectrum of  $\Lambda\Lambda$  generated from Eq. (1) with values that are given in Ref. 13 we obtain a threshold  $\Lambda\Lambda$  bump with a width of  $\sim 300 \text{ MeV}/c^2$ .  $\Lambda$  pairs which have an effective mass over  $100 \text{ MeV}/c^2$  above the  $\Lambda\Lambda$  threshold will in general point independently back toward the target without pointing through each other. On the other hand,  $\Lambda$  pairs with effective mass near the  $\Lambda\Lambda$  threshold will seem to come from a cascade of  $\Lambda$  decays. This fact will always make it very hard to find a neutral strangelet by this decay mode unless one has very good effective mass resolution. Things are much improved for the charge one strangelet, the requirement that an additional positive track must come from the first  $V$ , eliminates the bump. Figure 7d shows the effective mass spectrum for the  $\Lambda\Lambda p$  candidates and none have a mass below  $3.2 \text{ GeV}/c^2$  where the  $\Lambda\Lambda p$  threshold is  $3.17 \text{ GeV}/c^2$ . From this negative results, we claim that  $H_{\Lambda\Lambda}^3$  strangelet at the 90% confidence level must be produced at a rate less than  $2 \times 10^{-2}$  strangelets per central event if it had a lifetime around 3 nanoseconds and decayed only into the above decay channel.

## 6. CONCLUSIONS

Our  $K_s^0$  and  $\Lambda$  data are consistent with a slope behavior of  $B = a + b \cosh(y - y_0)$ , which is a form that comes from a fireball picture.[8] We have also shown that a scattering code can reproduce this fireball result if there are enough quick scatterings to effectively form a fireball. We have detected  $\Xi^-$ 's from  $Si Pb$  central events and find it is much larger than HIJET predicts. Finally, we have searched for strangelets that would decay in our TPC detector. Our experiment opens up the possibility to search for strangelets which have a lifetime that lies between the  $\Lambda$  lifetime and the 100 nanosecond lifetime of other experiments. We expect that our next experiment (E-891) to study  $11.5 \times A$  Gev/c  $Au$  on  $Au$  target, will have a better chance of detecting strangelets.

## ACKNOWLEDGEMENTS

We wish to thank the members of the AGS and MPS staff for their support during this experiment. Our special thanks go to E. Mogavero for her help during data analysis.

## REFERENCES

1. T. Abbott *et al.*, Phys. Rev. Lett. 64 (1990) 847; T. Abbott *et al.*, Phys. Rev. Lett. 66 (1991) 1567.
2. J. Barke *et al.*, Z. Phys. C48 (1990) 191.
3. S. Abatzis *et al.*, Phys. Lett. B244 (1990) 130; S. Abatzis *et al.*, Phys. Lett. B259 (1991) 508; S. Abatzis *et al.*, Phys. Lett. B270 (1991) 123.
4. S.E. Eiseman *et al.*, Phys. Lett. B248 (1990) 254.
5. J. Rafelski and R. Hagedorn, in: Thermodynamics of quarks and hadrons, ed. H. Satz (North Holland, Amsterdam, 1981).
6. C. Greiner, P. Koch and H. Stöcker, Phys. Rev. Lett. 58 (1987) 1825.
7. S.E. Eiseman *et al.*, Phys. Lett. B297 (1992) 44.
8. A. Bamberger *et al.*, Z. Phys. C38 (1988) 89; J. Stachel, Formation and Break-up of Hadronic Fireballs, in: Proc. of the Workshop on Heavy Ions at the AGS, (Brookhaven National Laboratory, March 1990), ed. O. Hansen, BNL-44911 (1990) 144.
9. V. Blobel *et al.*, Nucl. Phys. B69 (1974) 454.
10. R. Longacre, HIJET with AGS Physics and  $N^*$ 's, in: Proc. Heavy-Ion Physics at the AGS, (Massachusetts Institute of Technology, Jan. 1993), (eds.) G.S.F. Stephans, S.G. Steadman, and W.L. Kehoe, MITLNS-2158 (1993) 304.
11. J. Barrette *et al.*, Phys. Rev. C46 (1992) 312.
12. G. Baym and S.A. Chin, Phys. Lett. B62 (1976) 241; A. Chin and A.K. Kerman, Phys. Rev. Lett. 43 (1979) 1292; J.D. Bjorken and L.D. McLerran, Phys. Rev. D 20 (1979) 2353; E. Witten, Phys. Rev. D (1984) 272; E. Farhi and R.L. Jaffe, Phys. Rev. D (1984) 2379.
13. A.C. Saulys *et al.*, Neutral Strange Particle Production at the AGS, (Massachusetts Institute of Technology, Jan. 1993), (eds.) G.S.F. Stephans, S.G. Steadman, and W.L. Kehoe, MITLNS-2158 (1993) 196.